Electrochemical glucose biosensor based on ZnO nanorods modified with gold nanoparticles

Xiao Fen Hoo[1] · Khairunisak Abdul Razak[1,2] · Nur Syafinaz Ridhuan[1] · Noorhashimah Mohamad Nor[1] · Nor Dyana Zakaria[2]

Abstract

Gold nanoparticles (AuNPs) were synthesized by seeded-growth method. Spherical AuNPs with different sizes were formed by varying the volumes of the gold seed, hydroxylamine hydrochloride, and gold chloride. Zinc oxide nanorods (ZnONRs) were also produced through hydrothermal growth on seeded indium tin oxide (ITO) substrates. Zinc acetate sol seed was dropped onto the substrates, which were then oven dried at 150 °C. After heating the substrates at 500 °C for 2 h in a pre-heated tube furnace to obtain the ZnO seed, the substrates were immersed in a hydrothermal solution and heated at 80 °C for 4 h to obtain ZnONRs grown on ITO substrates. The synthesized AuNPs were then drop casted onto the ZnONR/ITO substrates, which were air dried to obtain AuNP/ZnONR/ITO electrodes. Glucose oxidase (GOx) enzyme and Nafion were subsequently dropped onto these modified electrodes. The electrochemical activity of the resulting Nafion/GOx/AuNP/ZnONR/ITO electrodes in glucose detection was evaluated through cyclic voltammetry. The size and volume of the AuNPs and the volume of GOx enzyme were found to influence the electrochemical activity. The optimized electrode consisting of Nafion, 60 μL of GOx, 80 μL of 30 nm AuNPs, ZnONRs, and ITO exhibited a low limit of detection of 0.18 mM and high sensitivities of 14.53 and 2.54 $\mu A \; mM^{-1} \; cm^{-2}$ within a wide working range of 0.05–1.0 and 1.0–20 mM, respectively.

1 Introduction

Diabetes mellitus is a metabolic disorder of multiple etiologies characterized by chronic hyperglycemia. It occurs because the human body fails to produce sufficient insulin or effectively utilize the produced insulin [1]. Strict control of diabetes can prevent or retard the progress of diabetes complications. If untreated properly, diabetes can affect pregnancy and cause other health problems, such as skin, eye, and foot complications, neuropathy, diabetes ketoacidosis and ketones, kidney diseases, hypertension, stroke, hyperosmolar hyperglycemic nonketonic syndrome, gastroparesis, heart diseases, and mental-health problems [2]. The glucose level of diabetic patients can be detected using a glucose sensor, which is a simple device that can be purchased at pharmacies. The working electrode of a test strip can be embedded with nanomaterials to provide a large surface area for enzymatic chemical reactions. The high surface-area-to-volume ratio of the nanomaterials leads to the large signal, good catalysis, and rapid movement of the analytes through the sensors [3].

The wide band gap of ZnO (3.37 eV) is attracting considerable attention for the development of Ultraviolet (UV) sensor [4], piezoelectric devices [5, 6], and biosensors [7–9]. ZnO nanostructures are characterized by nontoxicity, good electrochemical activity, and high electron-transfer ability. ZnO also has a high isoelectric point of approximately 9.5 and provides a positively charged substrate for the immobilization of glucose oxidase (GOx) enzymes with a low isoelectric point. Thus, ZnO is suitable for the modification of electrodes for glucose sensors. Meanwhile, gold (Au) nanostructures are catalytically active in glucose oxidation and are also potential materials for electrochemical glucose sensors [10]. Au nanostructures are stable, water soluble, optically sensitive, and biocompatible [11]. Given their large surface-to-volume ratio and the presence of active sites on their surface, Au nanoparticles (AuNPs) can be combined

✉ Khairunisak Abdul Razak
khairunisak@usm.my

1 School of Materials and Mineral Resources Engineering, Universiti Sains Malaysia, 14300 Nibong Tebal, Penang, Malaysia

2 NanoBiotechnology Research and Innovation (NanoBRI), Institute for Research in Molecular Medicine, Universiti Sains Malaysia, 11800 USM Penang, Malaysia

with zinc oxide nanorods (ZnONRs) to form nanocomposites for glucose-sensing applications. Indium tin oxide (ITO) substrate is industrially available at a considerably low cost, making it ideal for the mass fabrication of glucose sensors. This substrate also exhibits excellent optical transparency, high electrical conductivity, wide electrochemical working window, low capacitive current, and stability. Thus, ITO substrate is suitable for glucose sensors [12].

Many scholars have attempted to modify glucose sensors by using various Au/ZnO nanostructures, including Au-ZnONR hybrid nanocomposites [9], Au–ZnO bullet-like heterodimer nanoparticles [13], AuNPs and plant-like ZnO nanocomposite films [7], well-aligned ZnONRs by self-assembly deposited on AuNPs [14], and Au deposited on well-aligned ZnONRs by using a precision etching-coating system [15]. Chou et al. [14] fabricated ZnONR-modified AuNPs through chemical bath deposition to produce ZnONRs, followed by the self-assembly of AuNPs on ZnONR by soaking the ZnO electrode in AuNP colloidal solution. The fabricated electrode exhibits a poor catalytic activity. Chou et al. hypothesized that ZnO thin film does not grow homogenously. Different amounts of nanoparticles adhere onto the electrode, leading to poor catalytic activity that can also be due to the removal of ZnONRs from the electrode surface during glucose measurement caused by detachment from substrate [14]. Rahman et al. [16] posited that ZnO nanostructures have high sensitivity but poor stability because they are easily removed from the electrode surface during functionalization. Therefore, improving the stability of glucose sensors while maintaining or improving their sensitivity or selectivity remains a major challenge in glucose monitoring.

In the present work, well-aligned hydrothermally grown ZnONRs on ITO electrodes with drop-casted AuNPs for glucose biosensor application (AuNP/ZnONR/ITO) was performed. ZnONRs were grown on an ITO substrate with ZnO seeds through the hydrothermal method. The hydrothermal method offers a simple, cost-effective, and energy-efficient technique that requires a low growth temperature for the synthesis of ZnONRs with well-controlled morphology and growth direction [17, 18]. The glucose detection properties of all samples were found to be correlated with their structures and morphologies, indicating that good adhesion of AuNPs onto ZnONRs was another important factor affecting the properties of the glucose sensor. Various-sizes AuNPs prepared by seeded-growth method were drop casted onto ZnONR/ITO. The presence of the amine terminal group on the AuNPs promoted the good adherence of AuNPs onto the ZnONR surface. GOx is the most commonly used enzyme for fabricating biosensors because of its high sensitivity and good selectivity for glucose, simple acquisition, low-cost production, rapid response, and ability to withstand extreme pH, ionic strength, and temperature. These properties allow

relatively lax manufacturing and storage requirements [19, 20]. Nafion film was also used as a protective membrane to prevent enzyme loss and provide interference ability against other electroactive molecules. Several works have improved glucose detection by using hybrid AuNP/ZnONR [9, 14]; however, to the authors' knowledge, the effects of using various-sized AuNPs have not yet been comprehensively studied. Therefore, this work aimed to determine the optimum size of AuNPs decorated onto ZnONRs that can enable the most effective glucose detection.

2 Experimental details

2.1 Synthesis of ZnONR/ITO

ZnONRs were grown on ITO substrates with ZnO seeds through hydrothermal method. The 1 cm^2 ITO glass substrates were cleaned using Radio Corporation of America method to remove organic and inorganic contaminants. A mixture of water, ammonium hydroxide (NH$_4$OH, 29% purity), and hydrogen peroxide (H$_2$O$_2$, 30% purity) at a volume ratio of 20:4:1 was heated to 60 °C and maintained for 20 min. The ITO substrates were rinsed thrice with deionized (DI) water. Then, the ITO substrates were immersed in propanol ($\geq$ 99% purity) for 2 min and dried in an oven. Zinc acetate sol seed was prepared by dissolving 0.5 M zinc acetate dihydrate (ZnAc$_2\cdot$2H$_2$O, $\geq$ 99.5% purity) in methanol ($\geq$ 99.8% purity) and stirred vigorously at 60 °C for 20 min. Approximately 15 mL of ethanolamine (C$_2$H$_7$NO, $\geq$ 98% purity) was dropwise added to the solution as a stabilizer. The solution was stirred continuously at 60 °C for 2 h. The solution was aged at room temperature for 1 day prior to deposition. Approximately 10 μL of the seed was added onto the cleaned ITO glass substrate and heated at 150 °C for 20 min in an oven. This wetting procedure was repeated twice, and the sample was placed in a preheated tube furnace at 500 °C in air for 2 h to obtain ZnO seed layers. The ZnO seeds/ITOs were vertically immersed in hydrothermal growth solution containing 0.1 M zinc nitrate hexahydrate (Zn(NO$_3$)$_2\bullet$6H$_2$O, 98% purity) and 0.1 M hexamethylenetetramine (HMT, $\geq$ 99% purity) in screw-capped bottles and heated to 80 °C for 4 h to facilitate a hydrothermal reaction. The ITO substrates were removed from the screw-capped bottles and rinsed with DI water. The samples were placed on an aluminum dish and oven dried at 90 °C for 1 h.

2.2 Synthesis of AuNPs

Prior to synthesis of AuNPs, all glassware was cleaned with aqua regia solution with concentrated hydrochloric acid (HCl, $\geq$ 37% purity) and concentrated nitric acid (HNO$_3$, 65% purity) at a volume ratio of 3:1. Then, the equipment

was thoroughly washed with DI water to remove any residual aqua regia solution to avoid contamination. AuNPs were prepared by seeded-growth method, which involved two stages, namely, the Au seed preparation and the growth of Au seeds, as mentioned in our previous works [21, 22]. Au seed was synthesized by utilizing gold (III) chloride trihydrate ($HAuCl_4 \cdot 3H_2O$, 99.9% purity) as the gold precursor and trisodium citrate dihydrate ($Na_3C_6H_5O_7 \cdot 2H_2O$, $\geq$ 99% purity) as the reducing agent. Then, 125 mL of $HAuCl_4 \cdot 3H_2O$ (0.01% weight by volume (w/v)) was heated to boiling and continuously stirred at 350 rpm in an Erlenmeyer flask. The flask was covered with an aluminum foil to minimize evaporation. When the solution reached its boiling state, 2.5 mL of trisodium citrate (1% w/v) was added. The solution was stirred for 10 min to form 15 nm Au seeds. The solution color changed from light yellow to faint blue during this period. Over time, the solution changed from grayish blue to dark red, indicating the formation of AuNPs. After 10 min, the AuNP seed solution was removed from the heat source and continuously stirred for 5 min before being cooled to room temperature. At the growth stage, a certain volume of freshly prepared AuNP seed solution was added to 0.1 M of hydroxylamine hydrochloride ($NH_2OH \cdot HCl$, $\geq$ 99% purity) solution and stirred at 320 rpm for 5 min. Then, 25.4 mM of $HAuCl_4 \cdot 3H_2O$ was dropwise added into the solution at 10 s intervals between each drop. The stirring speed was increased to 350 rpm for 4–5 min to complete the reaction. The chemicals at the growth stage were tuned to obtain AuNPs of various sizes (Table 1).

2.3 Preparation of Nafion/GOx/AuNP/ZnONR/ITO modified electrode

AuNPs of various sizes and volumes were added on the ZnONR/ITO substrates. Sodium hydroxide (NaOH, $\geq$ 99% purity) was used to alter the pH of the AuNPs from acidic to neutral state before they were drop-casted onto ZnONR/ITO. The samples were dried at room temperature for 1 h. GOx solution was prepared by dissolving 1 mg of (50 k units/g) in 1 mL of 0.01 M phosphate buffer solution (PBS) and left overnight to stabilize the enzyme. Various volumes of GOx

were added onto the electrodes. Then, the electrodes were dried overnight at 8 °C. Approximately 20 μL of Nafion 117 (~ 5% in a mixture of lower aliphatic alcohols and water) solution was applied to the electrodes to eliminate any potential fouling and to prevent enzyme leaching. The electrodes were refrigerated at 4.0 °C when not in used.

2.4 Characterization

The particle size of the AuNPs was observed using transmission electron microscopy (TEM) (FEI CM12 Version 3.L image analysis system, 120 kV). The particle size distribution was evaluated by counting 100 nanoparticles in several TEM images by using ImageJ software. The hydrodynamic size and dispersity of the AuNPs were characterized using a Zetasizer particle size analyzer (Nanoseries Model ZEN3600, Malvern Instruments). The morphologies of the ZnONRs and the AuNP/ZnONR were observed through field-emission scanning electron microscopy (FESEM) (LEO Gemini 35VP). The phase presence was analyzed using X-ray diffraction (XRD) (Bruker D8). Cyclic voltammetry and amperometric measurements were performed using an electrochemical analyzer (Autolab) to observe the performance of the modified electrodes toward glucose. Electrochemical studies were conducted using a three-electrode setup, in which the sample served as the working electrode, a platinum wire served as the counter electrode, and Ag/AgCl served as the reference electrode in 0.01 M PBS for all measurements. The sensitivity of the Nafion/GOx/AuNP/ZnONR/ITO electrodes was evaluated by adopting various concentrations (0.1–20 mM) of glucose solution.

3 Results and Discussion

3.1 Characterization and morphology of AuNPs and ZnONR/ITO

AuNPs of various sizes were synthesized using seeded-growth method by varying the volume of AuNP seed solution as shown in TEM image in Fig. 1. The particle size

Table 1 Amount of chemicals used to synthesize AuNPs of various sizes and the results of TEM and zeta-sizer characterizations

Volume used to synthesize AuNPs (mL)			TEM		Zetasizer	
15 nm Au seed solution	0.1 M hydroxylamine hydrochloride	25.4 mM gold chloride	Average size (nm)	SD	Z-average (nm)	PDI
–	–	–	18 (seed)	2.36	20.82	0.087
120	12	6	25	3.58	29.97	0.372
63	9	4.5	30	5.06	42.61	0.096
28	7	3.5	37	8.48	44.16	0.112
8	4	2	45	6.06	58.78	0.102
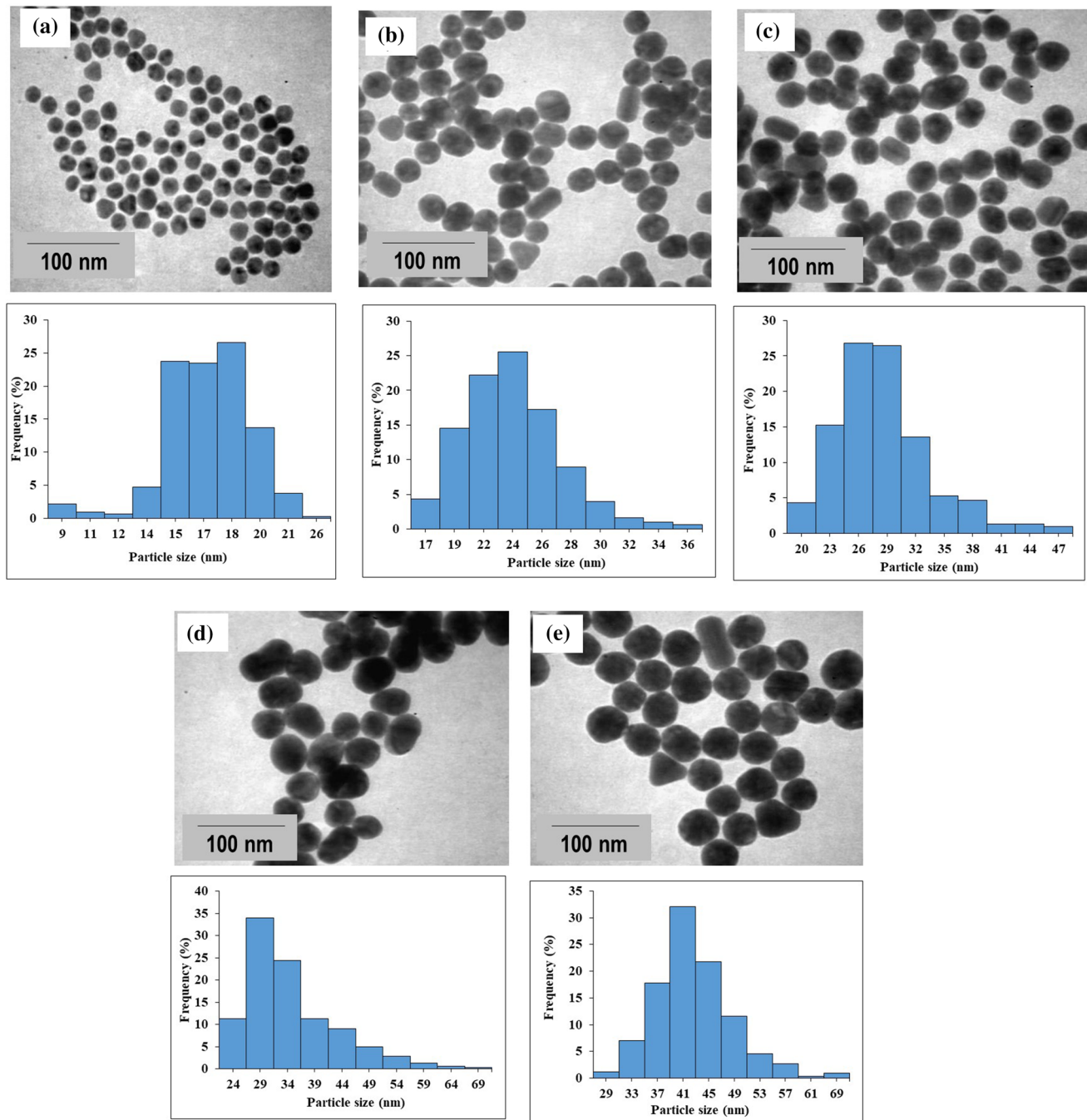
Fig. 1 TEM images and particle size histogram of **a** 18 nm Au seeds and AuNPs (with optical density of more than 3) synthesized using different volumes of Au seeds, $NH_2OH \cdot HCl$, and gold chloride (Table 1). The resulting sizes of AuNPs are as follows: **b** 25, **c** 30, **d** 37, and **e** 45 nm

distribution of the AuNPs from the TEM images was measured using ImageJ software and represented in the histograms. The average particle size of the Au seeds measured from the TEM images was 18 nm (Fig. 1a). The Au seeds were successfully grown to sizes of 25, 30, 37, and 45 nm (Fig. 1b–e). The homogeneity of the particle size distribution of the synthesized AuNPs is represented by the standard deviation measured from the particle size measurement of

the TEM images (Table 1). The standard deviation values of the particle size distribution were 2.36, 3.58, 5.06, 8.48, and 6.06 for 18 nm Au seeds and 25, 30, 37, and 45 nm AuNPs, respectively. Table 1 also lists the z-average and polydispersity index (PDI) value of the various sizes of AuNPs measured using the Malvern Zetasizer Nano-ZS. The z-average diameter is the mean hydrodynamic size of collection of particles measured via dynamic light scattering. Meanwhile,

the sample PDI represents the degree of non-uniformity of size distribution of AuNPs in solution [23]. The z-average for expected size 18, 25, 30, 37, and 45 nm AuNPs are 20.82, 29.97 42.61, 44.16, and 58.78 nm, respectively. The PDI for size 18, 25, 30, 37, and 45 nm AuNPs are 0.087, 0.372, 0.096, 0.112, and 0.102, respectively. Among these AuNPs, the 18, 30, 37, and 45 nm AuNPs are classified as narrowly monodisperse, whereas the 25 nm AuNPs is classified as moderate polydispersity.

XRD analysis was performed to verify the phase presence in the AuNP colloidal solution, and the results are shown in Fig. 2. Au patterns were observed at 38°, 44°, 65°, and 78°, which are corresponded to the (111), (200), (220), and

(311) planes of the face-centred cubic structure Au (ICDD 98-005-0876). The high intensity of the XRD patterns indicated the high crystallinities of Au and trace of sodium chloride (NaCl). The peaks at 32°, 46°, and 66° corresponded to the (200), (220), and (400) planes of NaCl (ICDD 98-008-1797), which was possibly produced by the chemicals used during synthesis.

As shown in Fig. 3a, ZnONRs were synthesized using seeded growth hydrothermal method following the optimum parameters established by Ridhuan et al. [17]. A large area of uniform ZnONRs with an average length and diameter of 767 and 151 nm, respectively, was formed using the selected hydrothermal parameters. The standard deviation

Fig. 2 XRD patterns of **a** bare glass, **b** 18 nm Au seeds, and **c** 25, **d** 30, **e** 37, and **f** 45 nm AuNPs
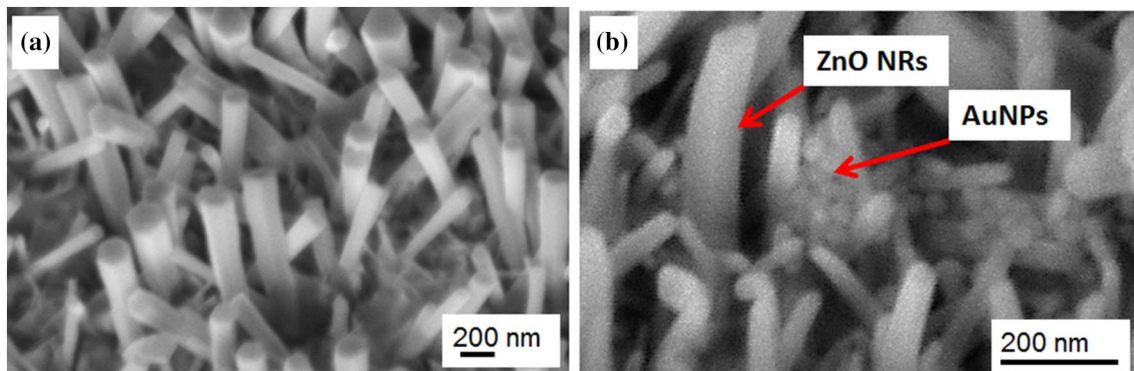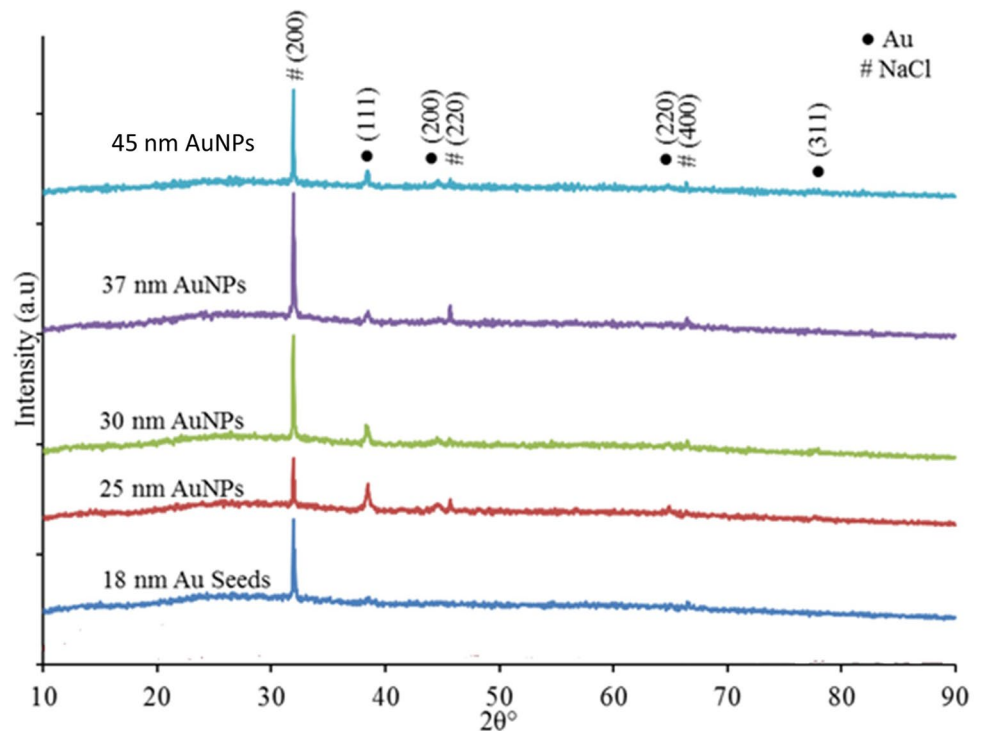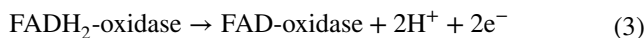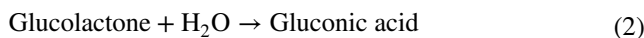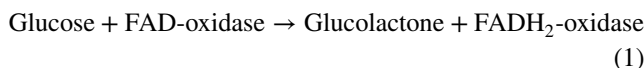

Fig. 3 FESEM image of the **a** uniform coverage of ZnONRs over large area and **b** AuNP-decorated ZnONRs via drop-casting method in 45° tilted view

of the average length and diameter were 115 and 35 nm, respectively. The produced AuNPs were drop-casted onto the grown ZnONRs and dried at room temperature for 1 h. As shown in Fig. 3b, AuNPs were successfully deposited on ZnONRs.

Figure 4 shows the XRD patterns of bare ITO, ZnONR/ITO, and AuNP/ZnONR/ITO of various sizes. The produced peaks matched with ZnO (zincite), Au, and ITO. The peaks at 32°, 35°, 37°, 48°, 57°, 64°, 67°, and 69° matched with zincite (ICDD: 98-010-5282), specifically for the (100), (002), (101), (102), (110), (103), (112), and (201) planes, respectively. Zincite has a hexagonal wurtzite crystal structure. The Au peak (ICDD: 98-005-0876) was located at 38°. The sharp peaks indicated that the fabricated AuNP/ZnONR/ITO had a high crystallinity. The Debye–Scherrer equation states that the peak broadness is inversely proportional to the crystalline size [24]. However, the differences in the peak broadness of the AuNPs of various sizes were not obvious because of the negligible differences in their sizes. Moreover, the amount of AuNPs was lower than that of ZnONRs, resulting in the low peak intensity of Au in the XRD patterns of AuNP/ZnONR/ITO, as shown in Fig. 4c–f. Hou et al. observed a similar XRD pattern [25]. The peaks at 31°, 36°, 51°, and 61° corresponded to the ITO substrate with a cubic structure (ICDD: 98-005-1985).

3.2 Electrocatalytic activity of varied size AuNP-modified ZnONR/ITO electrode

AuNPs of various sizes were drop-casted onto the fabricated ZnONR/ITO electrodes and tested for their properties as glucose sensors. The electrodes were air-dried at room temperature, immobilized with 20 μL of GOx, and protected with 20 μL of Nafion 117 solution. Figure 5 shows the cyclic voltammograms of the electrodes characterized in 0.01 M PBS with the presence of 10 mM glucose measured from $^-$1 to $+0.5$ V at an applied scan rate of 50 mV s^{-1}. No redox peak was observed for Nafion/GOx/ITO electrode because of the embedded flavin adenine dinucleotide (FAD) active site of GOx enzyme, which contributed to the difficulty of direct electron transfer between GOx enzyme and ITO electrode. As for Nafion/GOx/ZnONR/ITO-modified electrode, a pair well-defined oxidation peak at $^-0.37$ V potential was observed. The obtained results suggested that the catalytic reaction of the GOx enzyme immobilized on ZnONR surface toward glucose occurred as proposed in Eqs. (1)–(3):

$$\text{Glucose} + \text{FAD-oxidase} \rightarrow \text{Glucolactone} + \text{FADH}_2\text{-oxidase} \tag{1}$$

$$\text{Glucolactone} + \text{H}_2\text{O} \rightarrow \text{Gluconic acid} \tag{2}$$

$$\text{FADH}_2\text{-oxidase} \rightarrow \text{FAD-oxidase} + 2\text{H}^+ + 2\text{e}^- \tag{3}$$

Fig. 4 XRD patterns of **a** bare ITO, **b** ZnONR/ITO, **c** 25 nm AuNP/ZnONR/ITO, **d** 30 nm AuNP/ZnONR, **e** 37 nm AuNP/ZnONR/ITO, and **f** 45 nm AuNP/ZnONR/ITO
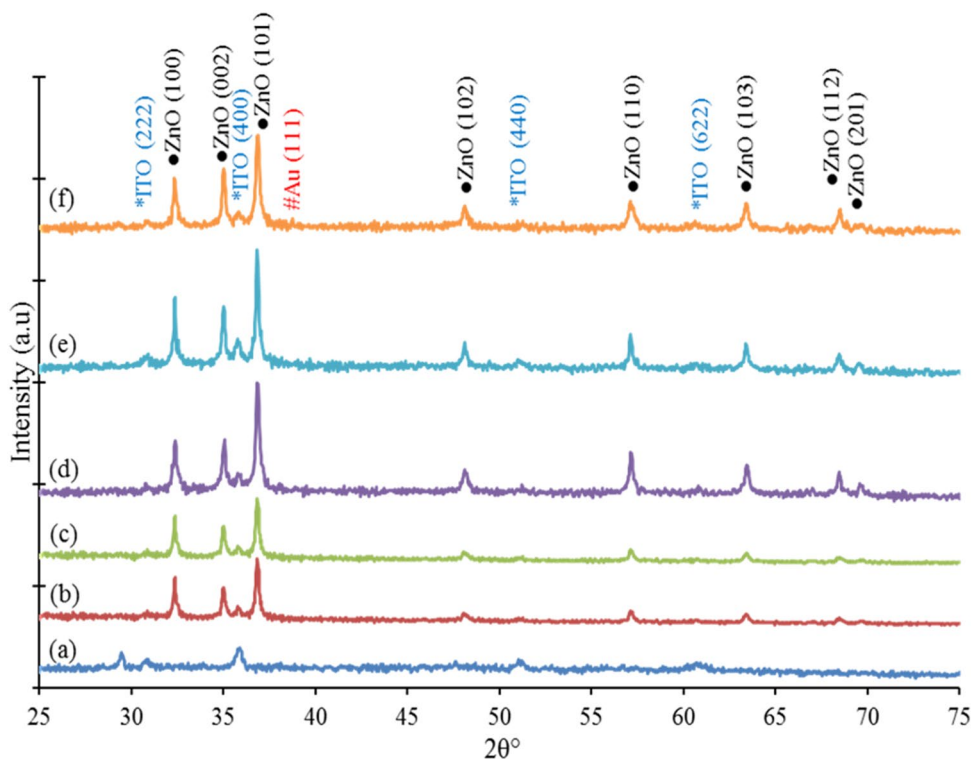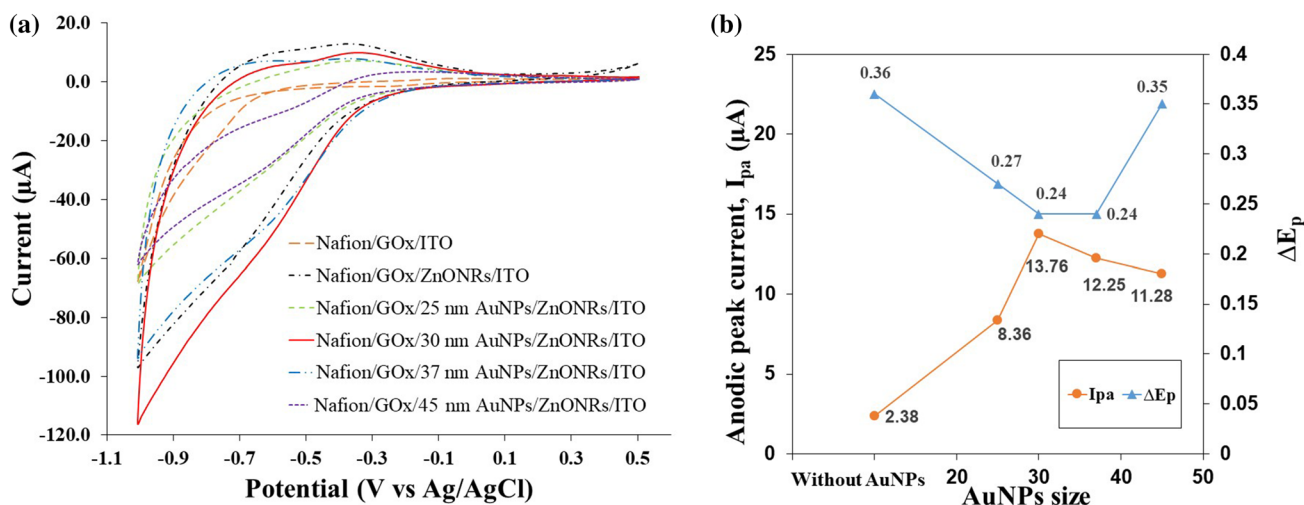
Fig. 5 **a** Cyclic voltammograms and **b** anodic peak current values and difference between cathodic and anodic peak potentials (ΔE_p) of AuNPs of various sizes on ZnONR/ITO in 0.01 mM PBS with presence of 10 mM glucose at a scan rate of 50 mV s^{-1}

where the FAD-oxidase served as the catalytic site of the GOx enzyme by receiving the electrons from the glucose oxidation reaction and being reduced to FADH$_2$-oxidase. In this process, glucose was converted into gluconolactone. Then, the FADH$_2$-oxidase was oxidized by the electrode to FAD-oxidase, where two protons and two electrons can subsequently transfer from GOx enzyme to Nafion/GOx/ZnONR/ITO-modified electrode.

The anodic peak current towards glucose significantly increased in Nafion/GOx/AuNPsZnONR/ITO-modified electrode than that Nafion/GOx/ZnONR/ITO-modified electrode (Fig. 5). Thus, the addition of AuNPs onto ZnONR/ITO improved the electrocatalytic activity of the modified electrode toward glucose. This performance was attributed to the large surface area available for GOx enzyme to immobilize on AuNP/ZnONR/ITO-modified electrode, also greatly improving the conductivity and the electron transfer capability. A similar finding was observed by other researchers for Au-modified plant-like nanorods and bullet-structured ZnO [9, 15, 16].

Among the AuNP/ZnONR/ITO electrodes, the electrode decorated with 30 nm AuNPs displayed the highest anodic peak current (13.76 μA). This observation can be due to the high surface area, low PDI (0.096), and good dispersion of the 30 nm AuNPs. The TEM images showed that the 30 nm AuNPs had a consistent round shape and a narrow size distribution. As for AuNP/ZnONR/ITO electrode decorated with 25 nm AuNPs, the anodic peak current showed the lowest value (8.36 μA) because of the decreased surface area for GOx enzyme immobilization due to the agglomeration of 25 nm AuNPs that revealed by high PDI value (0.372). As for AuNP/ZnONR/ITO electrode decorated with 37 and 45 nm AuNPs, slightly low anodic peak current values of

12.25 and 11.28 μA were obtained, respectively. This finding was due to the small surface area for GOx enzyme immobilization of AuNP/ZnONR/ITO electrode modified with the large AuNPs.

Cyclic voltammetry response also represents the reversibility redox reaction of the modified electrodes. The addition of AuNPs onto ZnONR/ITO significantly improved the reversibility of modified electrodes (Fig. 5b). These results were observed from the decrease in potential difference between cathodic and anodic peak potentials [ΔE_p ($E_{pc} - E_{pa}$)]. ΔE_p for Nafion/GOx//ZnONR/ITO electrode was 0.36 V, and Nafion/GOx/AuNP/ZnONR/ITO electrodes decorated with 25, 30, 37, and 45 nm were 0.27, 0.24, 0.24, and 0.35 V, respectively. The decrease in the value of peak potential difference between the anodic and cathodic peaks revealed fast electron transfer with the addition of AuNPs. This occurrence was due to the excellent electrical conductivity of AuNPs, facilitating the fast electron transfer in between the GOx enzyme and the AuNP/ZnONR/ITO-modified electrode. Similar finding was observed in Fang et al. [26], wherein AuNPs acted as the functional material for ZnO during modification of electrode for GOx enzyme immobilization. However, for ZnONR/ITO-modified electrode with 45 nm AuNPs, ΔE_p increased to 0.35 V because of the small surface area for GOx enzyme immobilization of AuNP/ZnONR/ITO electrode modified with the large AuNPs.

3.3 Effect of volume on AuNP-modified ZnONR/ITO

The effect of volume on the optimized size of AuNPs (30 nm) decorated on ZnONR/ITO was investigated in 0.01 M PBS in the presence of 10 mM glucose. The

obtained cyclic voltammograms are presented in Fig. 6. The sample with 80 µL of AuNPs exhibited the highest anodic and cathodic peak currents in response to glucose oxidation. The strongest electrocatalytic activity of 80 µL of AuNPs can be due to its ability to provide the maximum number of AuNPs attached on ZnONRs with the highest electrochemical surface area to accept a large number of electrons during glucose oxidation. At a low volume of AuNPs, the AuNPs cannot fully cover the ZnONRs, thereby causing insufficient active sites for reaction. At 100 µL, the AuNPs formed multiple layers or aggregated AuNPs, limiting their electrochemical reaction.

3.4 Effect of volume on GOx enzyme-modified ZnONR/ITO

After obtaining the optimum size (30 nm) and volume (80 µL) of AuNPs decorated on the ZnONR/ITO-modified electrode, optimization of GOx enzyme volumes immobilized on the AuNP/ZnONR/ITO is important to produce excellent electrocatalytic performance of the modified electrode. Figure 7 shows the cyclic voltammograms of various volumes of 20, 40, 60, 80, and 100 µL of 1 mg/mL GOx immobilized on the AuNP/ZnONR/ITO-modified electrodes. Electrodes without GOx and Nafion exhibited the highest anodic peak current (23.68 µA) than those with GOx
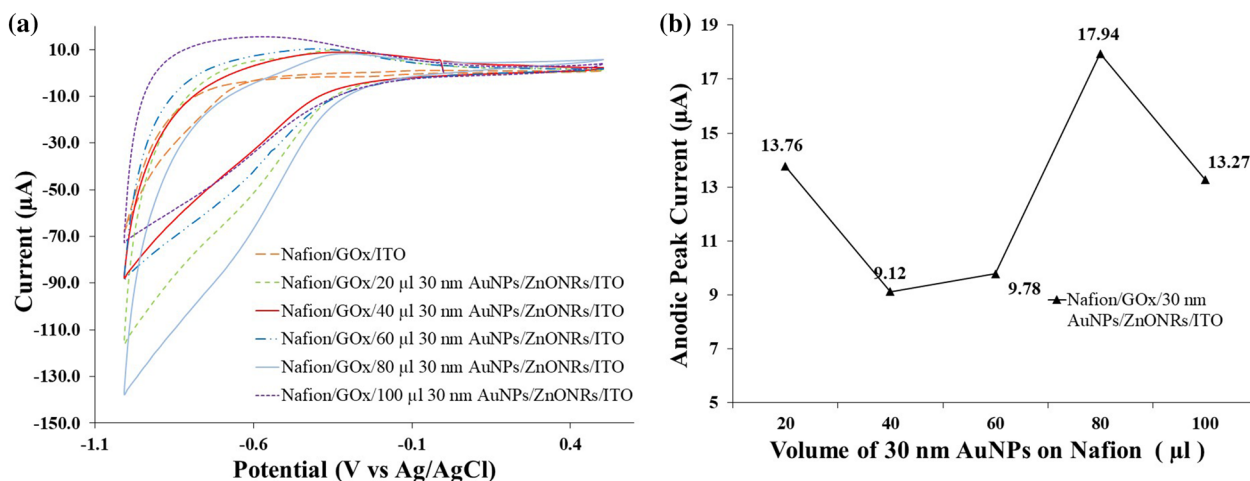
Fig. 6 **a** Cyclic voltammograms and **b** anodic peak current values of various volumes of 30 nm AuNPs on ZnONR/ITO in 0.01 mM PBS with presence of 10 mM glucose at a scan rate of 50 mV s^{-1}
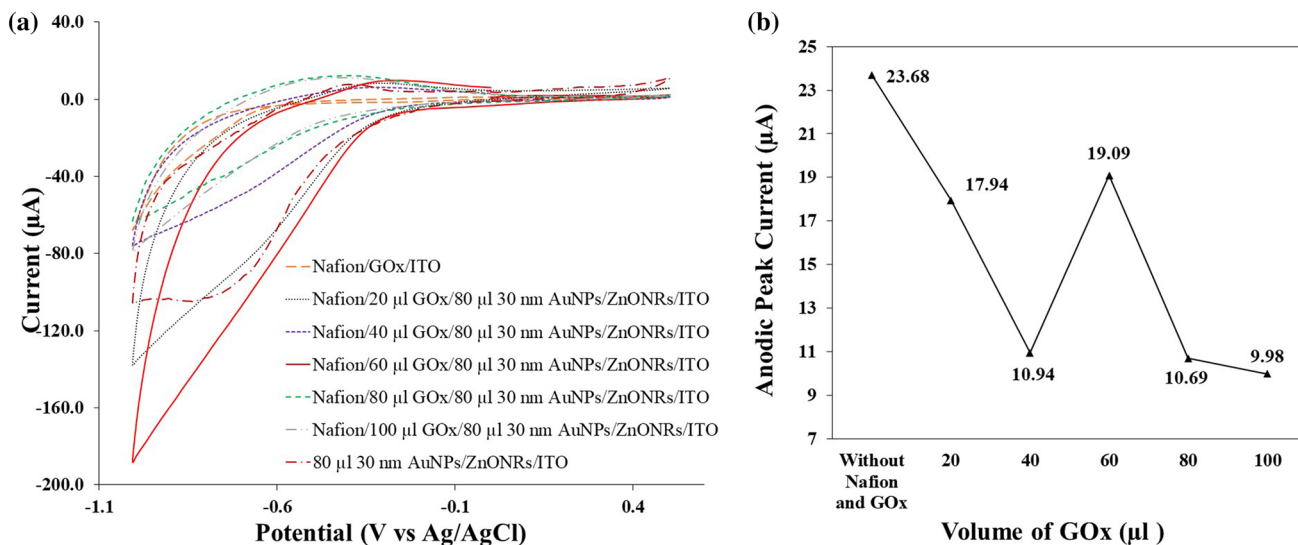
Fig. 7 **a** Cyclic voltammograms and **b** anodic peak current values of various volumes of GOx on 80 µL of 30 nm AuNP/ZnONR/ITO in 0.01 mM PBS with presence of 10 mM glucose at a scan rate of 50 mV s^{-1}

and Nafion. The Nafion layer acted as a protective layer that prevented the loss of enzyme molecules and improved the anti-interference ability of the glucose sensor [27]. However, the GOx and Nafion layers reduced the accessibility of glucose analytes and AuNP/ZnONR/ITO electrodes, which in turn reduced the anodic peak current. This finding agreed with the results of Chen et al. [28]. Nevertheless, the Nafion and GOx layers should be placed on the electrodes to catalyze the electrochemical reactions, prevent the GOx loss, and increase the glucose sensor selectivity.

Among the electrodes with various volumes of GOx, 60 μL of GOx showed the highest electrocatalytic activity. The anodic peak current for a GOx volume higher than 60 μL decreased slightly. The probable reason is that the excess GOx blocked the connection between the AuNPs and ZnONRs, hindering the electron transfer. For electrodes with GOx volume less than 60 μL, the GOx amount was insufficient for full functioning, resulting in a poor electrocatalytic activity.

3.5 Analytical performance of the modified electrode

Figure 8a presents the amperometric response of the Nafion/GOx/AuNP/ZnONR/ITO electrode at an applied potential of −0.5 V in 0.01 M PBS with the addition of glucose concentration ranging from 0.05 mM to 20 mM. The modified electrode demonstrated a rapid and sensitive response to changes in glucose concentration. Figure 8b shows the calibration curve between the current response and the glucose concentration. The current response displayed a good linear relationship with increased glucose concentration in

the range of 0.05–1.0 and 1.0–20 mM. The linear regression equations were $y_1 = 2.01 + 7.49x$ ($R^2 = 0.989$) and $y_2 = 7.10 + 1.32x$ ($R^2 = 0.993$) with sensitivities of 14.53 and 2.54 μA mM^{-1} cm^{-2}. The calculated limit of detection (LOD) was 0.18 mM. The electrode sensitivity and the detection limit of the modified electrode was calculated as shown in Eq. 4 [29] and Eq. 5 [30], as follows:

$$K = i/A \qquad (4)$$

where K is the electrode sensitivity (μA mM^{-1} cm^{-2}); i is the amperometric sensitivity (μA mM^{-1}), and A is the surface area (cm^{-2}) of the modified electrode. The amperometric sensitivity was obtained from the slope of the linear range calibration curves.

$$LOD = 3\sigma s/(3.3) \qquad (5)$$

where σ is the standard error of the regression line, and s is the slope of the calibration curve.

The fabricated electrode in this work showed a higher sensitivity of 2.54 μA mM^{-1} cm^{-2} compared with the electrodes produced by Chou et al. [14] (1.44 μA mM^{-1} cm^{-2}) and comparable with the electrodes produced by Tian et al. [7] (3.12 μA mM^{-1} cm^{-2}) (Table 2). The well-aligned ZnONRs allowed a better adhesion of AuNPs compared with those of plant-like Au-ZnO nanostructures by Tian et al. [7]. Chou et al. demonstrated that the poor catalytic activity was possibly due to the inhomogeneous ZnO thin film, which caused an uneven amount of AuNPs to adhere on the electrode [14]. The high catalytic response of the electrode in this work indicated that the drop-casted seeded-grown AuNPs and hydrothermally seeded-grown ZnONRs had considerable potential as glucose sensors. Although
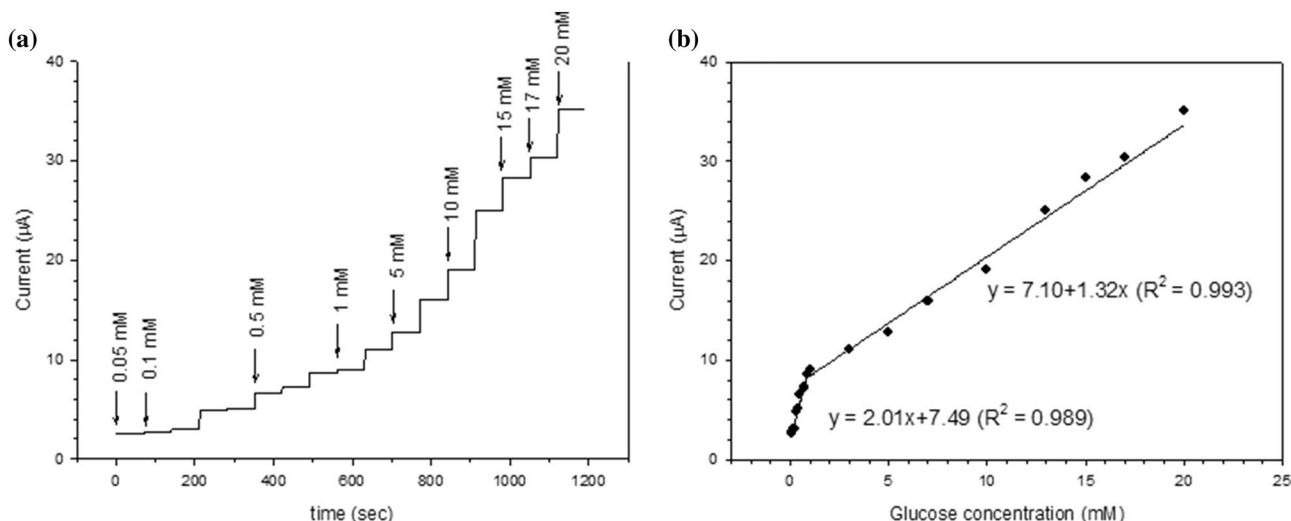
Fig. 8 **a** The amperometric current response, **b** The calibration curve between the amperometric current response and the glucose concentration of the Nafion/60 μL GOx/80 μL of 30 nm AuNP/ZnONR/ITO

electrode at an applied potential of −0.5 V in 0.01 M PBS with the addition of glucose concentration ranging from 0.05 to 20 mM

Table 2 Comparison among different Au–ZnO nanostructure electrodes from this work and previous work

Modified electrode	Sensitivity ($\mu A\ mM^{-1}\ cm^{-2}$)	LOD	Linear range	References
Nafion/GOx/Au ZnONRs hybrid /GCE/	1492	0.01 μM	0.1–33.0 μM	Wei et al. [9]
Au–ZnO/MWCNTs/GCE	44.7	0.19 μM	19–291 μM	Kumar et al. [13]
GOx/Au/ZnONRs/ITO	20.19	2 μM	Up to 20 mM	Bhattacharya et al. [15]
GOx/AuNPs/ZnO/ITO	3.12	N/A	2.78–22.22 mM	Tian et al. [7]
GOx/ZnONRs/AuNPs/ ITO	1.44	3510 mM	1.38–22.22 mM	Chou et al. [14]
Nafion/GOx/AuNPs/ZnONRs/ITO	14.53	0.18 mM	0.05–1.0 mM	This work
	2.54		0.1–20 mM	

the calculated sensitivity was lower than that of the Au/ZnO nanostructure glucose sensor studied by Wei et al. [9] (1492 $\mu A\ mM^{-1}\ cm^2$), Kumar et al. [13] (44.7 $\mu A\ mM^{-1}\ cm^2$), and Bhattacharya et al. [15] (20.19 $\mu A\ mM^{-1}\ cm^2$), the working range of glucose sensor in this work (0.05–20 mM) was higher than that of Wei et al. [9] (0.1–33.0 μM) and Kumar et al. [13] (19–291 μM). The normal blood glucose ranges of 4–8 mM [31] and the narrow linear range of the electrodes produced in their works are difficult to detect. Details on the glucose sensors are presented in Table 2. As shown in Fig. 8b, the electrode displayed a range of linearity at 0.05–1 and 1–20 mM. However, a slight deviation from the linearity was observed at 1 mM glucose. Under normal conditions, a deviation from linearity occurs frequently at high glucose concentrations. At a high glucose level, the rate of oxygen delivery into the sensor begins to surpass the rate of oxygen replenishment, thereby preventing the relative recovery of oxygen levels within the sensor [32]. Nevertheless, this change was not observed in Fig. 8b. Instead, the linear response deviated at low glucose concentrations. In conclusion, the Nafion/GOx/AuNP/ZnONR/ITO electrode exhibited a low LOD of 0.18 mM and high sensitivity value of 14.53 and 2.54 $\mu A\ mM^{-1}\ cm^{-2}$ in wide working range of 0.05–1.0 and 1.0–20 mM, respectively.

Selectivity is one of the important factors in glucose sensors as easily oxidative species, such as ascorbic acid (AA), uric acid (UA) and L-cysteine (L-Cys) compounds, typically co-existing with glucose in human blood. The electrochemical response of interference species to the glucose oxidation was investigated. Figure 9 shows that the addition of 0.1 mM each of the interfering species in 1 mM of glucose slightly increased the current response. The current response increased to 0.57% (Glu + AA), 1.22% (Glu + UA), and 2.44% (Glu + L-Cys) with respect to the current response to 1 mM glucose. These values were calculated using Eq. (6) as follows [33]:

$$\%\ Interference = \left[(I_X - I_O)/I_O\right] \times 100 \tag{6}$$

where I_X is the current response of 1 mM glucose solution with interfering species presence, and I_O is the current
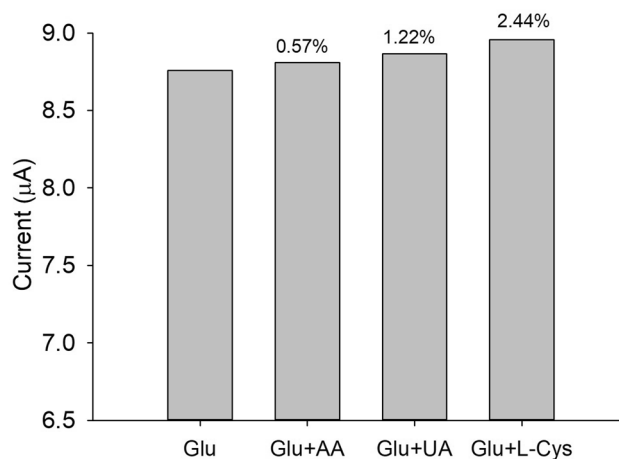
Fig. 9 The electrochemical response of 0.1 mM interference species of AA, UA and L-Cys in 1 mM of glucose

response of 1 mM glucose solution. The Nafion/GOx/AuNP/ZnONR/ITO electrode had good selectivity toward glucose detection. The use of Nafion layer served as an effective permeable selective barrier to minimize the interferences [34]. The negatively charged sulfonate (SO_3^-) groups in Nafion prevented the negatively charged interfering species from penetrating into the electrode surface. This finding has also been observed by other authors [9, 12].

Figure 10 illustrates the schematic of glucose detection by electrochemical method by using AuNP-decorated ZnONR-modified ITO electrodes. The use of AuNP-decorated ZnONRs increased the surface area and the dynamics, facilitating a direct electron transfer between the enzyme and the modified electrode. The structure of the AuNP-decorated ZnO can entrap and encompass GOx enzymes, thereby contributing to direct electron transfer from the GOx enzymes to the modified electrode. The presence of combined spherical AuNPs and ZnONR structure in nanoscale also contributed to the good electron transfer between the enzyme and the modified electrode. Moreover, the use of AuNPs can provide an electrical pathway that would facilitate a good electron
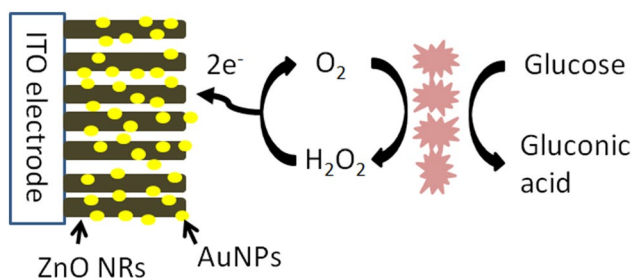
Fig. 10 Schematic of glucose detection by electrochemical method by using AuNP-decorated ZnONR-modified ITO electrode

transfer. In addition, AuNPs exhibit electrocatalytic activity and are the most stable metal nanoparticles apart from Pt and Ag nanoparticles [35]. AuNPs can attach to many biological molecules, making them ideal for fabricating biosensors as they provide a good matrix for attaching GOx enzymes while retaining the original properties [35]. Therefore, the use of AuNP-decorated ZnO nanorods increased the generated output current signal, which was proportional to the glucose concentration through the direct electron transfer from GOx to the modified electrode.

4 Conclusion

Nafion/GOx/AuNP/ZnONR/ITO was successfully fabricated. AuNPs of various sizes were successfully synthesized by seeded-growth method. ZnONRs were fabricated by seeded hydrothermal method. AuNPs of different sizes were drop-casted on the prepared ZnONR/ITO substrates. GOx and Nafion were added on the prepared AuNP/ZnONR/ITO electrode. The optimized condition modification of electrode was Nafion/60 µL GOx/80 µL of 30 nm AuNP/ZnONR/ITO, exhibiting high sensitivity of 14.53 and 2.54 $\mu A\ mM^{-1}\ cm^{-2}$ for a wide working range of 0.05–1.0 and 1.0–20 mM and a low LOD of 0.18 mM. Thus, AuNP/ZnONR is an attractive material for fabricating efficient amperometric glucose sensors.

References

1. K.G.M.M. Alberti, P.Z. Zimmet, Diabet. Med. **15**, 539–553 (1998)
2. K.J. Cash, H.A. Clark, Trends Mol. Med. **16**, 584–593 (2010)
3. M. Taguchi, A. Ptitsyn, E.S. McLamore, J.C. Claussen, J. Diabetes Sci. Technol. **8**, 403–411 (2014)
4. C. Fu, K.J. Lee, K. Lee, S.S. Yang, Smart Mater. Struct. **24**, 015010 (2015)
5. T.S. Van Den Heever, W.J. Perold, Smart Mater. Struct. **22**, 105029 (2013)
6. L. Chenchen, H. Shuling, S. Shengping, Smart Mater. Struct. **21**, 115024 (2012)
7. K. Tian, S. Alex, G. Siegel, A. Tiwari, Mater. Sci. Eng. C **46**, 548–552 (2015)
8. C. Karuppiah, M. Velmurugan, S.-M. Chen, S.-H. Tsai, B.-S. Lou, M. Ajmal, Ali, F.M.A. Al-Hemaid, Sensors Actuators B **221**, 1299–1306 (2015)
9. Y. Wei, Y. Li, X. Liu, Y. Xian, G. Shi, L. Jin, Biosensors Bioelectron. **26**, 275–278 (2010)
10. L.Y. Chen, X.Y. Lang, T. Fujita, M.W. Chen, Scr. Mater. **65**, 17–20 (2011)
11. L. Sun, D. Zhao, Z. Song, C. Shan, Z. Zhang, B. Li, D. Shen, J. Colloid Interface Sci. **363**, 175–181 (2011)
12. Y. Fu, F. Liang, H. Tian, J. Hu, Electrochim. Acta **120**, 314–318 (2014)
13. D.R. Kumar, D. Manoj, J. Santhanalakshmi, RSC Adv. **4**, 8943–8952 (2014)
14. H.T. Chou, J.H. Lin, H.C. Hsu, T.M. Wu, C. Liu, Int. J. Electrochem. Sci. **10**, 519–528 (2015)
15. C. Bhattacharya, V.P. Jain, Rao, S. Banerjee, in *AIP Conference Proceedings*, vol. 1447 (2012), pp. 295–296
16. M.M. Rahman, A.J.S. Ahammad, J.-H. Jin, S.J. Ahn, J.-J. Lee, Sensors **10**, 4855–4886 (2010)
17. N.S. Ridhuan, K. Abdul Razak, Z. Lockman, A. Abdul Aziz, PLoS ONE **7**, e50405 (2012)
18. N.S. Ridhuan, K. Abdul, Razak, Z. Lockman, Sci. Rep. **8**, 13722 (2018)
19. E.-H. Yoo, S.-Y. Lee, Sensors **10**, 4558–4576 (2010)
20. A.P. Periasamy, Y.-J. Chang, S.-M. Chen, Bioelectrochemistry **80**, 114–120 (2011)
21. M. Siti Rabizah, R. Khairunisak Abdul, N. Rahmah, Z. Nor Dyana, C. Tan Soo, Nanotechnology **23**, 495719 (2012)
22. X.-F. Hoo, K.A. Razak, N.S. Ridhuan, N.M. Nor, N.D. Zakaria, in *AIP Conference Proceedings*, vol. 1877 (2017), p. 030001
23. K.N. Clayton, J.W. Salameh, S.T. Wereley, T.L. Kinzer-Ursem, Biomicrofluidics **10**, 054107 (2016)
24. R. Yogamalar, R. Srinivasan, A. Vinu, K. Ariga, A.C. Bose, Solid State Commun. **149**, 1919–1923 (2009)
25. X. Hou, L. Wang, G. He, J. Hao, CrystEngComm. **14**, 5158–5162 (2012)
26. L. Fang, B. Liu, L. Liu, Y. Li, K. Huang, Q. Zhang, Sensors Actuators B **222**, 1096–1102 (2016)
27. L. Ambrozy, Hlavata, J. Labuda, Acta Chim. Slovoca **6**, 35–41 (2013)
28. K.-J. Chen, C.-F. Lee, J. Rick, S.-H. Wang, C.-C. Liu, B.-J. Hwang, Biosensors Bioelectron. **33**, 75–81 (2012)
29. S. Jin, C.C. Jonathan, S.M. Eric, H. Aeraj ul, J. David, R.D. Alfred, C.-M. Percy, L.R. Jenna, D.M. Porterfield, Nanotechnology **22**, 355502 (2011)
30. A. Shrivastava, V. Gupta, Chron. Young Sci. **2**, 21–25 (2011)
31. A.E.G. Cass, G. Davis, G.D. Francis, H.A.O. Hill, Anal. Chem. **56**, 667–669 (1984)
32. D. Bruen, C. Delaney, L. Florea, D. Diamond, Sensors (Basel, Switzerland) **17**, 1866 (2017)
33. G. Aydoğdu, D.K. Zeybek, Ş. Pekyardimci, E. Kiliç, Artif. Cells Nanomed. Biotechnol. **41**, 332–338 (2013)
34. L. Zhang, S. Yuan, L. Yang, Z. Fang, G.-C. Zhao, Microchim. Acta **180**, 627–633 (2013)
35. A.A. Saei, J.E.N. Dolatabadi, P. Najafi-Marandi, A. Abhari, M. de la Guardia, Trends Anal. Chem. **42**, 216–227 (2013)